

PandA: Unsupervised Learning of Parts and Appearances in the Feature Maps of GANs

James Oldfield¹Christos Tzelepis¹Yannis Panagakis²Mihalis A. Nicolaou³Ioannis Patras¹¹School of Electronic Engineering and Computer Science, Queen Mary University of London²Dept. of Informatics and Telecommunications, University of Athens³Computation-based Science and Technology Research Center, The Cyprus Institute

Abstract

Recent advances in the understanding of Generative Adversarial Networks (GANs) have led to remarkable progress in visual editing and synthesis tasks, capitalizing on the rich semantics that are embedded in the latent spaces of pre-trained GANs. However, existing methods are often tailored to specific GAN architectures and are limited to either discovering global semantic directions that do not facilitate localized control, or require some form of supervision through manually provided regions or segmentation masks. In this light, we present an architecture-agnostic approach that jointly discovers factors representing spatial parts and their appearances in an entirely unsupervised fashion. These factors are obtained by applying a semi-nonnegative tensor factorization on the feature maps, which in turn enables context-aware local image editing with pixel-level control. In addition, we show that the discovered appearance factors correspond to saliency maps that localize concepts of interest, without using any labels. Experiments on a wide range of GAN architectures and datasets show that, in comparison to the state of the art, our method is far more efficient in terms of training time and, most importantly, provides much more accurate localized control. Our code is available at: <https://github.com/james-oldfield/PandA>.

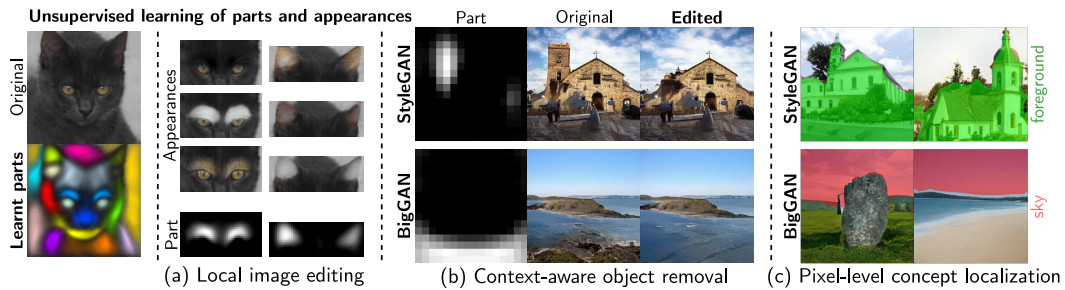


Figure 1: We propose an unsupervised method for learning a set of factors that correspond to interpretable parts and appearances in a dataset of images. These can be used for multiple tasks: (a) local image editing, (b) context-aware object removal, and (c) producing saliency maps for learnt concepts of interest.

1 Introduction

Generative Adversarial Networks (GANs) [17] constitute the state of the art (SOTA) for the task of image synthesis. However, despite the remarkable progress in this domain through improvements to the image generator’s architecture [46, 27, 30, 31, 29, 6], their inner workings remain to a large extent unexplored. Developing a better understanding of the way in which high-level concepts are represented and composed to form synthetic images is important for a number of downstream tasks such as generative model interpretability [47, 3, 57] and image editing [20, 49, 48, 53, 52, 2]. In modern generators however, the synthetic images are produced through an increasingly complex interaction of a set of per-layer latent codes in tandem with the feature maps themselves [31, 30, 29] and/or with skip connections [6]. Furthermore, given the rapid pace at which new architectures are being developed, demystifying the process by which these vastly different networks model the constituent parts of an image is an ever-present challenge. Thus, many recent advances are architecture-specific [55, 11, 39] and a general-purpose method for analyzing and manipulating convolutional generators remains elusive.

A popular line of GAN-based image editing research concerns itself with learning so-called “interpretable directions” in the generator’s latent space [20, 49, 48, 53, 52, 57, 21, 18, 19]. Once discovered, such representations of high-level concepts can be manipulated to bring about predictable changes to the images. One important question in this line of research is how latent representations are combined to form the appearance at a particular *local* region of the image. Whilst some recent methods attempt to tackle this problem [54, 55, 5, 63, 62, 39, 26], the current state-of-the-art methods come with a number of important drawbacks and limitations. In particular, existing techniques require prohibitively long training times [55, 63], costly Jacobian-based optimization [63], and the requirement of semantic masks [55] or manually specified regions of interest [63]. Furthermore, whilst these methods [63, 55] successfully find directions affecting local changes, optimization must be performed on a per-region basis, and the resulting directions do not provide *pixel-level* control [63].

In this light, we present a fast unsupervised method for *jointly* learning factors for interpretable parts and their appearances (we thus refer to our method as *Panda*) in pre-trained convolutional generators. Our method allows one to both interpret and edit an image’s style at discovered local semantic regions of interest, using the learnt appearance representations. We achieve this by formulating a constrained optimization problem with a semi-nonnegative tensor decomposition of the dataset of deep feature maps $\mathcal{Z} \in \mathbb{R}^{M \times H \times W \times C}$ in a convolutional generator. This allows one to accomplish a number of useful tasks, prominent examples of which are shown in Fig. 1. Firstly, our learnt representations of appearance across samples can be used for the popular task of local image editing [63, 55] (for example, to change the colour or texture of a cat’s ears as shown in Fig. 1 (a)). Whilst the state-of-the-art methods [63, 55] provide fine-grained control over a target region, they adopt an “annotation-first” approach, requiring an end-user to first manually specify a ROI. By contrast, our method fully exploits the unsupervised learning paradigm, wherein such concepts are discovered automatically and without any manual annotation. These discovered semantic regions can then be chosen, combined, or even modified by an end-user as desired for local image editing.

More interestingly still, through a generic decomposition of the feature maps our method identifies representations of common concepts (such as “background”) in *all* generator architectures considered (all 3 StyleGANs [30, 31, 29], ProgressiveGAN [27], and BigGAN [6]). This is a surprising finding, given that these generators are radically different in architecture. By then editing the feature maps using these appearance factors, we can thus, for example, *remove* specific objects in the foreground (Fig. 1 (b)) in all generators, seamlessly replacing the pixels at the target region with the background appropriate to each image.

However, our method is useful not only for local image editing, but also provides a straightforward way to localize the learnt appearance concepts in the images. By expressing activations in terms of our learnt appearance basis, we are provided with a *visualization* of how much of each of the appearance concepts are present at each spatial location (i.e., saliency maps for concepts of interest). By then thresholding the values in these saliency maps (as shown in Fig. 1 (c)), we can localize the learnt appearance concepts (such as sky, floor, or background) in the images—without the need for supervision at any stage.

We show exhaustive experiments on 5 different architectures [31, 27, 29, 30, 6] and 5 datasets [12, 7, 30, 60, 28]. Our method is not only orders of magnitude faster than the SOTA, but also

Table 1: A high-level comparison of our method to the SOTA for local image editing. “Training time” denotes the total training time required to produce the images for the quantitative comparisons.

	Manual ROI-free	Semantic mask-free	Pixel-level control	Architecture-agnostic	Style diversity	Training time (mins)
StyleSpace [55]	✓	✗	✗	✗	✓	177.12
LowRankGAN [63]	✗	✓	✗	✓	✗	392.97
Ours	✓	✓	✓	✓	✓	0.87

showcases superior performance at the task of local image editing, both qualitatively and quantitatively. Our contributions can be summarized as follows:

- We present an architecture-agnostic unsupervised framework for learning factors for both the parts and the appearances of images in pre-trained GANs, that enables local image editing. In contrast to the SOTA [63, 55], our approach requires neither semantic masks nor manually specified ROIs, yet offers more precise pixel-level control.
- Through a semi-nonnegative tensor decomposition of the generator’s feature maps, we show how one can learn sparse representations of semantic parts of images by formulating and solving an appropriate constrained optimization problem.
- We show that the proposed method learns appearance factors that correspond to semantic concepts (e.g., background, sky, skin), which can be localized in the image through saliency maps.
- A rigorous set of experiments show that the proposed approach allows for more accurate local image editing than the SOTA, while taking only a fraction of the time to train.

2 Related work

Generative Adversarial Networks (GANs) [17] continue to push forward the state of the art for the task of image synthesis through architectural advances such as the use of convolutions [46], progressive growing [27], and style-based architectures [30, 31, 29]. Understanding the representations induced by these networks for interpretation [3, 47, 57] and control [48, 47, 49, 20, 53, 15, 52, 63, 55, 1] has subsequently received much attention.

However, whilst several methods identify ways of manipulating the latent space of GANs to bring about global semantic changes—either in a supervised [16, 44, 48, 47] or unsupervised [53, 49, 20, 52, 42] manner—many of them struggle to apply *local* changes to regions of interest in the image. In this framework of local image editing, one can swap certain parts between images [11, 24, 8, 50, 32, 2], or modify the style at particular regions [54, 55, 5, 63, 62, 39, 26]. This is achieved with techniques such as clustering [11, 62, 5, 26], manipulating the AdaIN [23] parameters [55, 54], or/and operating on the feature maps themselves [54, 5, 62] to aid the locality of the edit. Other approaches employ additional latent spaces or architectures [32, 39], require the computation of expensive gradient maps [54, 55] and semantic segmentation masks/networks [55, 64, 39], or require manually specified regions of interest [63]. In contrast to related work, our method automatically learns both the parts and a diverse set of global appearances, in a fast unsupervised procedure without any semantic masks. Additionally, our method allows for *pixel-level* control [63]: the ability to *precisely* target specific pixels in the image. For example, one can choose to modify a single eye only in a face, which is not possible with the SOTA [63]. Our method and its relationship to the SOTA for local image editing is summarized in Table 1.

From a methodological standpoint, most closely related to our method are the works of Collins et al. [11, 10]. Both of these perform clustering in the activation space for parts-based representations in generators [11] and CNNs [10] respectively. However, [10] considers only discriminative networks for locating common semantic regions in CNNs, whilst we additionally focus on image editing tasks in GANs. On the other hand, [11] does not jointly learn representations of *appearances*. Therefore [11] is limited to “part swapping”, and is additionally StyleGAN-specific, unlike our method.

3 Methodology

In this section, we detail our approach for jointly learning interpretable parts and their appearances in pre-trained GANs, in an unsupervised manner. We begin by establishing the notation used throughout

factorization of the form

$$\mathbf{Z}_{i(3)} = \mathbf{A}\mathbf{A}_i\mathbf{P}^\top \quad (1)$$

$$= \underbrace{\begin{bmatrix} | & & | \\ \mathbf{a}_1 & \cdots & \mathbf{a}_{R_C} \\ | & & | \end{bmatrix}}_{\text{Appearance}} \underbrace{\begin{bmatrix} \lambda_{i11} & \lambda_{i12} & \cdots \\ \vdots & \ddots & \\ \lambda_{iR_C1} & \cdots & \lambda_{iR_C R_S} \end{bmatrix}}_{\text{Sample } i\text{'s coefficients}} \underbrace{\begin{bmatrix} - & \mathbf{p}_1^\top & - \\ \vdots & & \\ - & \mathbf{p}_{R_S}^\top & - \end{bmatrix}}_{\text{Parts}}, \quad (2)$$

where $\mathbf{A} \in \mathbb{R}^{C \times R_C}$ are the global appearance factors and $\mathbf{P} \geq \mathbf{0} \in \mathbb{R}^{S \times R_S}$ are the global parts factors, jointly learnt across many samples in a dataset. Intuitively, the coefficients λ_{ijk} encode how much of appearance \mathbf{a}_j is present at part \mathbf{p}_k in sample i 's feature maps $\mathbf{Z}_{i(3)}$. We show our proposed separable decomposition schematically in Fig. 2. Each *non-negative* parts factor $\mathbf{p}_k \in \mathbb{R}^S \geq \mathbf{0}$ spans a spatial sub-region of the feature maps, corresponding to a semantic part. The various appearances and textures present throughout the dataset are encoded in the appearance factors $\mathbf{a}_j \in \mathbb{R}^C$ and lie along the depth-wise channel mode of the feature maps. This formulation facilitates modelling the multiplicative interactions [25] between the parts and appearance factors. Concretely, due to the outer product, the factors relating to the parts control the spatial regions at which the various appearance factors are present. The parts factors thus function similarly to semantic masks, but rather are learnt jointly and in an entirely unsupervised manner. This is particularly useful for datasets for which segmentation masks are not readily available.

3.3 Objective

We propose to solve a constrained optimization problem that leads to the two desirable properties outlined in Section 3.2. We impose hard non-negativity constraints on the parts factors \mathbf{P} to achieve property 1, and encourage both factor matrices to be column-orthonormal for property 2 (which has been shown to lead to sparser representations [14, 58, 59, 61], and has intricate connections to clustering [13, 37]). We achieve this by formulating a single reconstruction objective as follows. Let $\mathcal{Z} \in \mathbb{R}^{N \times C \times S}$ be a batch of N samples' mode-3 unfolded intermediate activations. Then our constrained optimization problem is

$$\min_{\mathbf{A}, \mathbf{P}} \mathcal{L}(\mathcal{Z}, \mathbf{A}, \mathbf{P}) = \min_{\mathbf{A}, \mathbf{P}} \sum_{i=1}^N \|\mathbf{Z}_i - \mathbf{A}(\mathbf{A}^\top \mathbf{Z}_i \mathbf{P})\mathbf{P}^\top\|_F^2 \quad \text{s.t. } \mathbf{P} \geq \mathbf{0}. \quad (3)$$

A good reconstruction naturally leads to orthogonal factor matrices (e.g., $\mathbf{P}^\top \mathbf{P} \approx \mathbf{I}_{R_S}$ for $\mathbf{P} \in \mathbb{R}^{S \times R_S}$ with $S \geq R_S$) without the need for additional hard constraints [35]. What's more, each parts factor (column of \mathbf{P}) is encouraged to span a distinct spatial region to simultaneously satisfy both the non-negativity and orthonormality-via-reconstruction constraints. However, this problem is non-convex. We thus propose to break the problem into two sub-problems in \mathbf{A} and \mathbf{P} separately, applying a form of block-coordinate descent [38], optimizing each factor matrix separately whilst keeping the other fixed. The gradients of the objective function in Eq. (3) with respect to the two factor matrices (see the supplementary material for the derivation) are given by

$$\nabla_{\mathbf{P}} \mathcal{L} = 2 \left(\sum_{i=1}^N \bar{\mathbf{P}} \mathbf{Z}_i^\top \bar{\mathbf{A}} \bar{\mathbf{A}} \mathbf{Z}_i \mathbf{P} + \mathbf{Z}_i^\top \bar{\mathbf{A}} \bar{\mathbf{A}} \mathbf{Z}_i \bar{\mathbf{P}} \mathbf{P} - 2 \mathbf{Z}_i^\top \bar{\mathbf{A}} \mathbf{Z}_i \mathbf{P} \right), \quad (4)$$

$$\nabla_{\mathbf{A}} \mathcal{L} = 2 \left(\sum_{i=1}^N \bar{\mathbf{A}} \mathbf{Z}_i \bar{\mathbf{P}} \bar{\mathbf{P}} \mathbf{Z}_i^\top \mathbf{A} + \mathbf{Z}_i \bar{\mathbf{P}} \bar{\mathbf{P}} \mathbf{Z}_i^\top \bar{\mathbf{A}} \mathbf{A} - 2 \mathbf{Z}_i \bar{\mathbf{P}} \mathbf{Z}_i^\top \mathbf{A} \right), \quad (5)$$

with $\bar{\mathbf{P}} \triangleq \mathbf{P} \mathbf{P}^\top$ and $\bar{\mathbf{A}} \triangleq \mathbf{A} \mathbf{A}^\top$. After a gradient update for the parts factors \mathbf{P} , we project them onto the non-negative orthant [38] with $\max\{\mathbf{0}, \cdot\}$. This leads to our alternating optimization algorithm, outlined in Algorithm 1.

Upon convergence of Algorithm 1, to modify an image i at region k with the j^{th} appearance with desired magnitude $\alpha \in \mathbb{R}$, we compute the forward pass from layer l onwards in the generator with $\mathcal{X}'_i = G_{[l:]}(\mathbf{Z}_i + \alpha \mathbf{a}_j \hat{\mathbf{p}}_k^\top)$, with $\hat{\mathbf{p}}_k$ being the normalized parts factor of interest.

Algorithm 1: Block-coordinate descent solution to Eq. (3)

Input : $\mathcal{Z} \in \mathbb{R}^{M \times C \times S}$ (M lots of mode-3-unfolded activations), $R_C, R_S \in \mathbb{R}$ (ranks),
 $\lambda \in \mathbb{R}$ (learning rate), and T (# iterations).
Output : $\mathbf{P} \in \mathbb{R}^{S \times R_S}$, $\mathbf{A} \in \mathbb{R}^{C \times R_C}$ (*parts* and *appearance* factors).
Initialise
 $\mathbf{U}, \Sigma, \mathbf{V}^\top \leftarrow \text{SVD} \left(\mathbf{Z}_{(2)} \mathbf{Z}_{(2)}^\top \right)$;
 $\mathbf{A}^{(1)} \leftarrow \mathbf{U}_{:R_C}$;
 $\mathbf{P}^{(1)} \sim \mathcal{U}(0, 0.01)$;
for $t = 1$ **to** T **do**
 $\mathbf{P}^{(t+1)} \leftarrow \max \left\{ \mathbf{0}, \mathbf{P}^{(t)} - \lambda \cdot \nabla_{\mathbf{P}^{(t)}} \mathcal{L} \left(\mathcal{Z}, \mathbf{A}^{(t)}, \mathbf{P}^{(t)} \right) \right\}$; // PGD step
 $\mathbf{A}^{(t+1)} \leftarrow \mathbf{A}^{(t)} - \lambda \cdot \nabla_{\mathbf{A}^{(t)}} \mathcal{L} \left(\mathcal{Z}, \mathbf{A}^{(t)}, \mathbf{P}^{(t+1)} \right)$;
end

3.4 Initialization

Let $\mathcal{Z} \in \mathbb{R}^{N \times C \times S}$ be a batch of N mode-3 unfolded feature maps as in Section 3.3. A common initialization strategy [9, 4, 61] for non-negative matrix/tensor decompositions is via a form of HOSVD [51, 40]. Without non-negativity constraints, the channel factor matrix subproblem has a closely related closed-form solution given by the first R_C left-singular vectors of the mode-2 unfolding of the activations expressed in terms of the parts basis (proof given in Appendix B of [56]). We thus initialize the channel factors at time-step $t = 1$ with $\mathbf{A}^{(1)} \triangleq \mathbf{U}_{:R_C}$ where $\mathbf{U}_{:R_C}$ are the first R_C -many left-singular vectors of $\mathbf{Z}_{(2)} \mathbf{Z}_{(2)}^\top$. Later on in Section 4.1.2 we demonstrate the benefits of this choice, including its usefulness for locating interpretable appearances.

3.5 Parts factors refinement

The formulation in Eq. (3) for learning parts and appearances makes the implicit assumption that the samples are spatially aligned. However, this does not always hold in practice, and therefore the global parts are not always immediately useful for datasets with no alignment. To alleviate this requirement, we propose a fast optional “refinement” step of the global parts factors $\mathbf{P} \in \mathbb{R}^{S \times R_S}$ from Eq. (3) to specialize them to sample-specific parts factors $\tilde{\mathbf{P}}_i \in \mathbb{R}^{S \times R_S}$ for sample i . Given the i^{th} target sample’s intermediate activations $\mathbf{Z}_i \in \mathbb{R}^{C \times S}$, we optimize a few steps of a similar constrained optimization problem as before:

$$\min_{\tilde{\mathbf{P}}_i} \mathcal{L}_R(\mathbf{Z}_i, \mathbf{A}, \tilde{\mathbf{P}}_i) = \min_{\tilde{\mathbf{P}}_i} \|\mathbf{Z}_i - \mathbf{A} \left(\mathbf{A}^\top \mathbf{Z}_i \tilde{\mathbf{P}}_i \right) \tilde{\mathbf{P}}_i^\top\|_F^2 \quad \text{s.t. } \tilde{\mathbf{P}}_i \geq \mathbf{0}. \quad (6)$$

We analyze in Section 4.3.2 the benefits of this refinement step, and compare the global parts factors to the refined factors.

4 Experiments

In this section we present a series of experiments to validate the method and explore its properties. We begin in Section 4.1 by focusing on using the method for interpretation: showing how one can generate saliency maps for concepts of interest and remove the foreground at target locations. Following this, we showcase local image editing results on 5 GANs in Section 4.2. Finally, we present ablation studies in Section 4.3 to further justify and motivate our method.

4.1 Interpreting the appearance vectors

Using the learnt appearance basis \mathbf{A} , one can straightforwardly visualize “how much” of each column is present at each spatial location via a change of basis. In particular, the element at row c and column s of the activations expressed in terms of the appearance basis $\mathbf{A}^\top \mathbf{Z}_i \in \mathbb{R}^{R_C \times S}$ encodes how much of appearance c is present at spatial location s , for a particular sample i of interest. This transformation

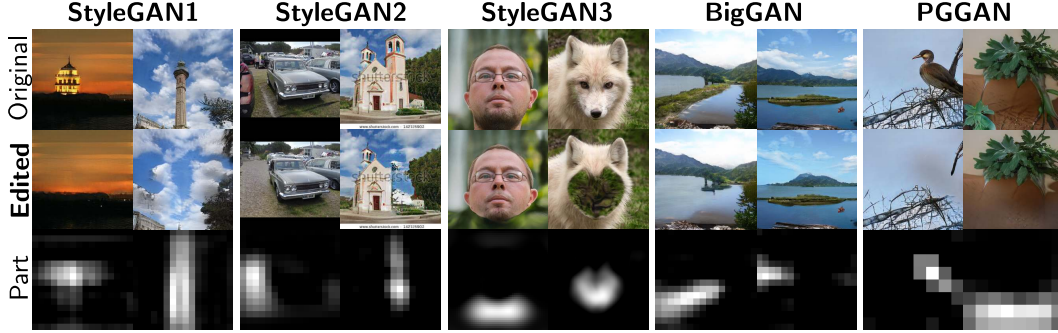


Figure 3: Our architecture-agnostic method discovers a representation of the “background” concept directly in the feature maps, which allows us to remove objects in a context-aware manner in the same way for all 5 generators.

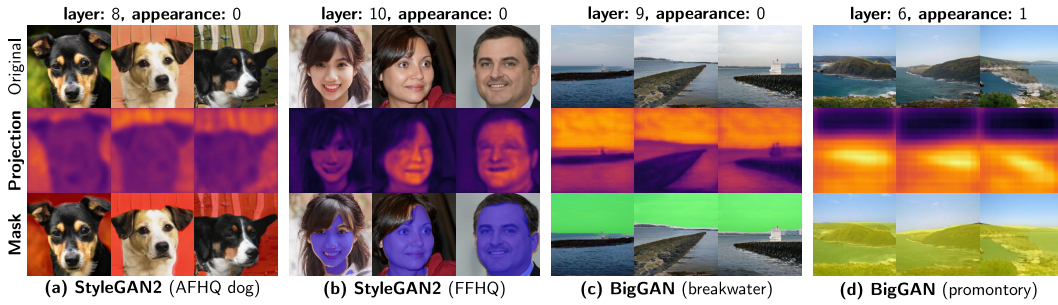


Figure 4: Visualizing the coordinates in the appearance basis (2nd row), one can interpret how much of each appearance vector is present at each spatial patch. For example, we see appearance vectors at various layers very clearly corresponding to (a) background, (b) skin, (c) sky, and (d) foreground.

provides a visual understanding of the concepts controlled by the columns by observing the semantic regions in the image at which these values are the highest.

4.1.1 Generic concepts shared across GAN architectures

The analysis above leads us to make an interesting discovery. We find that our model frequently learns an appearance vector for a high-level “background” concept in *all* 5 generator architectures. This is a surprising finding—one would not necessarily expect these radically different architectures to encode concepts in the same manner (given that many existing methods are architecture-specific), let alone that they could be extracted with a single unsupervised approach. We can thus use this learnt “background” appearance vector to remove objects in a context-aware manner, as shown on all 5 generators and numerous datasets in Fig. 3.

4.1.2 Visualizing and localizing appearance vectors

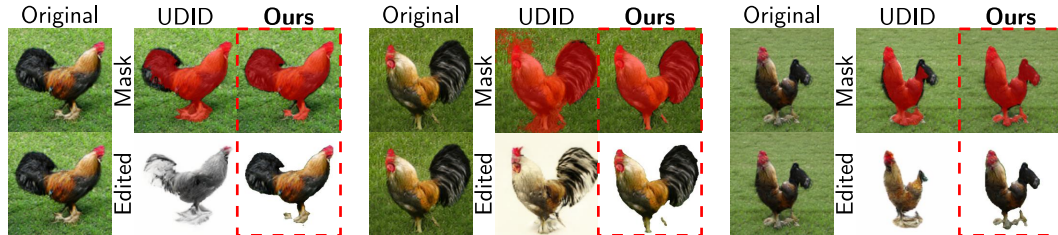


Figure 5: A comparison of our method to [53] for background removal and object detection: we leave the object of interest largely untouched.

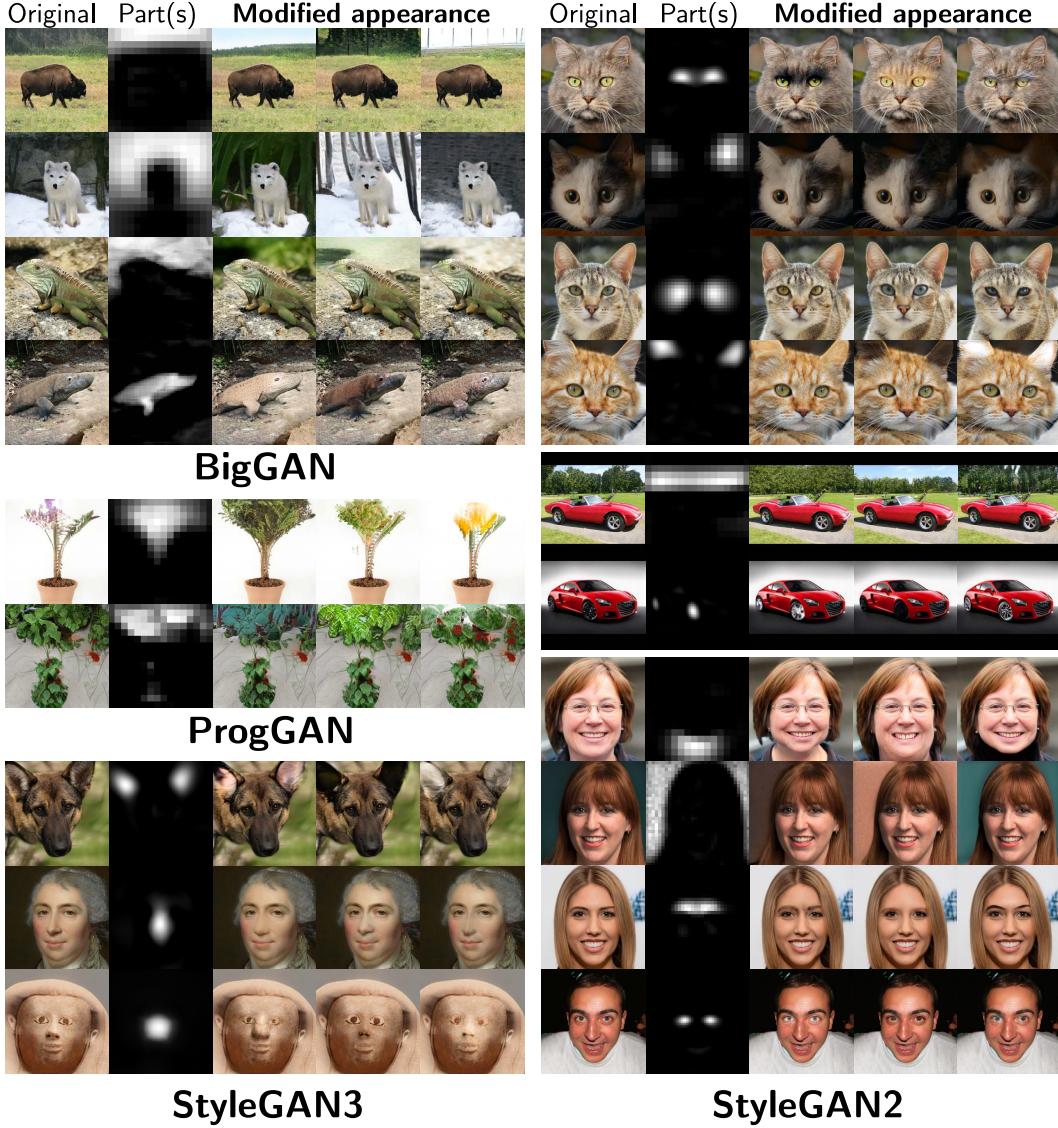


Figure 6: Local image editing on a number of architectures and datasets, using both the global and refined parts factors. At each column, the original image is edited at the target part with a different appearance vector.

Through the change of basis $\mathbf{A}^\top \mathbf{Z}_i$ we can identify the pixels in the image that are composed of the concept k of interest (e.g., the “background” concept), offering an interpretation of the images’ semantic content. We first compute the saliency map $\mathbf{m}_{ik} = \mathbf{a}_k^\top \mathbf{Z}_i \in \mathbb{R}^S$, whose elements encode the magnitude of concept k at each spatial position in the i^{th} sample. This can be reshaped into a square matrix and visualized as an image to localize the k^{th} concept in the image, as shown in row 2 of Fig. 4. We then additionally perform a simple binary classification following [53]. We classify each pixel j as an instance of concept k or not with $\tilde{m}_{ikj} = [m_{ikj} \geq \mu_k]$, where $\mu_k = \frac{1}{N \cdot S} \sum_{n,s} m_{nks} \in \mathbb{R}$ is the mean magnitude of the k^{th} concept in N samples. We show this in row 3 of Fig. 4 for various datasets and GANs. For example, this analysis allows us to identify (and localize) appearance vectors in various generators that control concepts including “foreground”, “skin”, and “sky”, shown in Fig. 4 (b-d). We find this visualization to be most useful for understanding the first few columns of \mathbf{A} , which control the more prominent high-level visual concepts in the dataset due to our SVD-based initialization outlined in Section 3.4.

Prior work [53] identifies a “background removal” interpretable direction in the latent space of BigGAN. By using our thresholded saliency maps for the “background” concept as a mask at the pixel-level, we can straightforwardly perform background *removal*, as shown in Fig. 5. As can be seen, our method can remove the background whilst successfully leaving the image untouched, whereas [53] often drastically modifies the foreground. More importantly, unlike [53], we can use our method to localize or remove any of the concepts encoded in the columns of our appearance basis, in addition to the background.

4.2 Local image editing

Next, we showcase our method’s ability to perform local image editing in pre-trained GANs, on 5 generators and 5 datasets (ImageNet [12], AFHQ [7], FFHQ [30], LSUN [60], and MetFaces [28]). In Fig. 6 we show a number of interesting local edits achievable with our method, using both the global and refined parts factors. Whilst we can manipulate the style at common regions such as the eyes with the global parts factors, the refined parts factors allow one to target regions such as an individual’s clothes, or their background. One is not limited to this set of learnt parts however. For example, one can draw a ROI by hand at test-time or modify an existing part—an example of this is shown in the supplementary material. This way, pixel-level control (e.g., opening only a single eye of a face) is achievable in a way that is not possible with the SOTA methods [63, 55].

We next compare our method to state-of-the-art GAN-based image editing techniques in Fig. 7. In particular, we train our model at layer 5 using $R_S = 8$ global parts factors, with no refinement. As can be seen, SOTA methods such as LowRank-GAN [63] excel at enlarging the eyes in a photo-realistic manner. However, we frequently find the surrounding regions to change as well. This is seen clearly by visualizing the mean squared error [11] between the original images and their edited counterparts, shown in every second row of Fig. 7. We further quantify this ability to affect local edits in the section that follows.

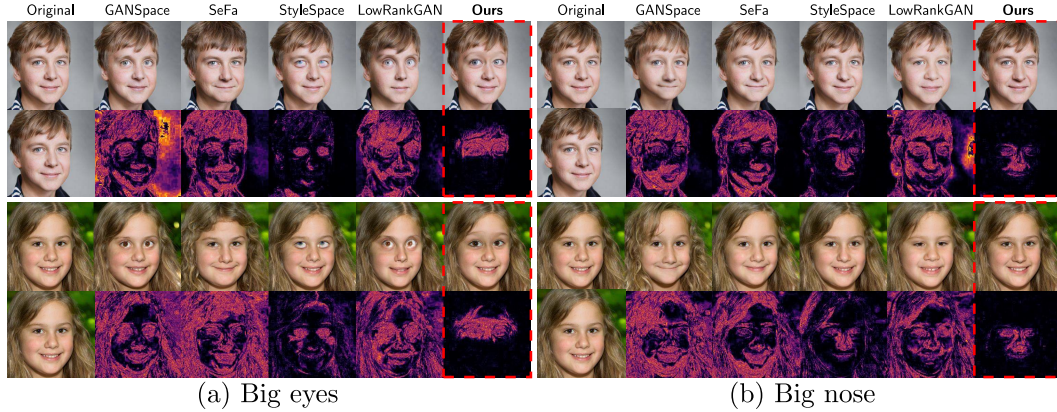


Figure 7: Qualitative comparison to SOTA methods editing the (a) eyes and (b) nose ROI. We also show the mean squared error [11] between the original images and their edited counterparts, highlighting the regions that change.

4.2.1 Quantitative results

We compute the ratio of the distance between the pixels of the original and edited images in the region of ‘disinterest’, over the same quantity with the region of interest (call it ROIR). Concretely, we compute

$$\text{ROIR}(\mathcal{M}, \mathcal{X}, \mathcal{X}') = \frac{1}{N} \sum_{i=1}^N \frac{\|(\mathbf{1} - \mathcal{M}) * (\mathcal{X}_i - \mathcal{X}'_i)\|}{\|\mathcal{M} * (\mathcal{X}_i - \mathcal{X}'_i)\|}, \quad (7)$$

where $\mathcal{M} \in [0, 1]^{H \times W \times C}$ is an $H \times W$ spatial mask (replicated along the channel mode) specifying the region of interest, $\mathbf{1}$ is a 1-tensor, and $\mathcal{X}, \mathcal{X}' \in \mathbb{R}^{N \times \tilde{H} \times \tilde{W} \times \tilde{C}}$ are the batch of original and edited versions of the images respectively. A small ROIR indicates more ‘local’ edits, through desirable

Table 2: ROIR (\downarrow), FID (\downarrow) [22] and SWD (\downarrow) [45] for 1k FFHQ samples.

	Eyes			Nose			Open mouth			Smile		
	ROIR	FID	SWD	ROIR	FID	SWD	ROIR	FID	SWS	ROIR	FID	SWD
SeFa [49]	5.02	14.97	120.71	6.82	13.21	115.56	3.50	25.03	183.32	4.05	18.50	117.40
GANSpace [20]	3.42	13.61	172.21	4.95	14.45	85.35	3.26	51.12	204.46	3.12	21.35	183.77
StyleSpace [55]	1.34	7.24	69.12	1.68	6.93	41.99	1.25	14.83	99.68	2.07	9.05	72.54
LowRankGAN [63]	1.81	14.55	131.53	5.06	14.53	89.90	1.84	19.91	134.84	2.35	13.54	138.60
Ours	1.13	6.04	54.42	1.25	5.33	61.87	1.12	8.24	77.84	1.12	7.10	48.41

change to the ROI (large denominator) and little change elsewhere (small numerator). We compute this metric for our method and SOTA baselines in Table 2, for a number of regions of interest. As can be seen, our method consistently produces more local edits than the SOTA for a variety of regions of interest. We posit that the reason for this is due to our operating directly on the feature maps, where the spatial activations have a direct relationship to a patch in the output image. We also show these images’ quality is SOTA by computing both FID [22] and SWD [45] metrics in Table 2.

4.3 Ablation studies

In this subsection, we present a thorough study of the various parts of our method, and the resulting learnt parts factors.

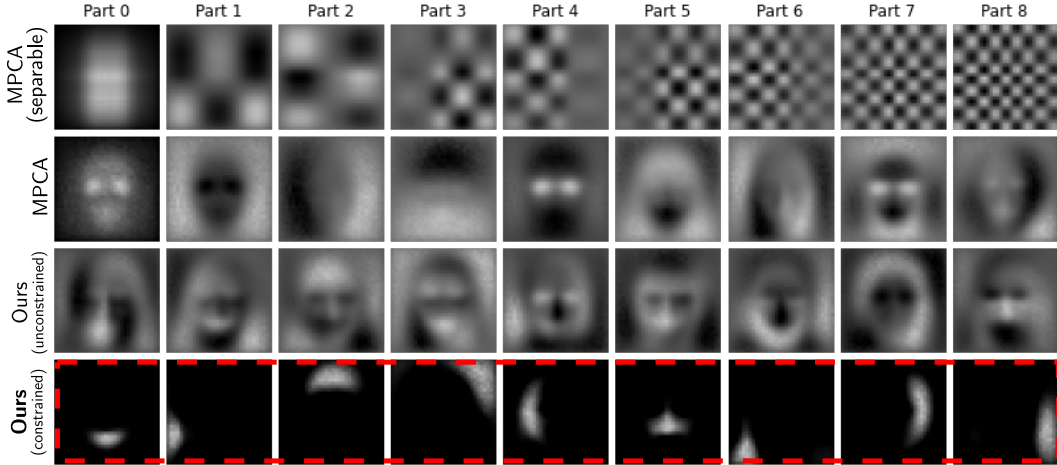


Figure 8: Ablation study comparing the parts factors learnt with various constraints and formulations. As can be seen, only our constrained formulation learns factors that span local parts-based semantic regions.

4.3.1 Constraints and form

We first study the impact of the non-negativity constraints on the parts factors, and the importance of operating on the mode-3 unfolded $\mathbf{Z}_{i(3)} \in \mathbb{R}^{C \times H \times W}$ tensors (rather than their original 3rd-order form $\mathcal{Z}_i \in \mathbb{R}^{H \times W \times C}$). We show along the rows of Fig. 8 the resulting parts factors using various forms of decomposition and constraints. In particular, naively applying MPCA [40] (row 1) to decompose \mathcal{Z}_i imposes a separable structure *between* the spatial modes, restricting its ability to capture semantic spatial regions. Moreover, even when combining the spatial modes and decomposing $\mathbf{Z}_{i(3)}$, the solution given by MPCA [40] (row 2) and by optimizing our method *without* any non-negativity constraints (row 3) leads to parts factors spanning the entire spatial window. This is due to the non-additive nature of the parts. However, as shown in row 4 of Fig. 8, only our constrained method successfully finds local, non-overlapping semantic regions of interest.

4.3.2 Parts factors refinement

Finally, we showcase the benefit of our optional parts factors refinement process for data with no alignment. In row 2 of Fig. 9, we show the global parts factors overlaid over the target samples. Clearly, for extreme poses (or in the case of data with no alignment, such as with animals and cars), these global parts will not correspond perfectly to the specific sample’s parts (row 2 of Fig. 9). However, after a few projected gradient descent steps of Eq. (6), we see (row 3 of Fig. 9) that the refined parts factors span the specific parts of the individual samples more successfully. This refinement step is very fast; for example, at $l = 6$ it takes only 127ms (100 iterations).



Figure 9: Visualization of the global parts factors (middle row) and the refined factors (bottom row) for particular samples (top row).

4.3.3 Training time

An important benefit of our method is the lack of need to compute expensive gradient maps or Jacobians with respect to target regions [63, 55]. To quantify this, we benchmark the total time needed to train the methods to produce the results in Table 2. This is summarized in Table 1 (and shown in detail in the supplementary material). We find that our method takes less than $1/400^{\text{th}}$ of the training time of LowRankGAN [63], and $1/170^{\text{th}}$ the time of StyleSpace [55]—greatly speeding up the task of local image editing.

Alternatively, one can use an optimizer such as Adam [33] in an autograd framework (e.g., PyTorch [43]) to compute Algorithm 1. We find this removes some sensitivity to the learning rate that comes with vanilla gradient descent. However, we find that when solving our objective manually with the gradients in Eq. (5), our method takes less than $1/3^{\text{rd}}$ of the time to train. This is a particularly useful performance boost when decomposing later layers in the network.

5 Conclusion

In this paper, we have presented a fast unsupervised algorithm for learning interpretable parts and their appearances in pre-trained GANs. We have shown experimentally how our method outperforms the state of the art at the task of local image editing, in addition to being orders of magnitude faster to train. We showed how one can identify and manipulate generic concepts in 5 generator architectures for tasks such as object removal. We also believe that our method’s ability to visualize the learnt appearance concepts through saliency maps could be a useful tool for network interpretability.

5.1 Limitations

Whilst we have demonstrated that our method can lead to more precise control, the approach is not without its limitations. For example, we find that the tendency to introduce artifacts is greater with methods editing the feature maps, relative to methods working on the latent codes. This is one potential risk with the freedom of pixel-level control—adding appearance vectors at arbitrary spatial locations does not always lead to photorealistic edits. We hope to address this in future work.

References

- [1] Abdal, R., Zhu, P., Mitra, N.J., Wonka, P.: StyleFlow: Attribute-conditioned exploration of StyleGAN-generated images using conditional continuous normalizing flows. *ACM Trans. Graph.* **40**(3) (May 2021)
- [2] Bau, D., Liu, S., Wang, T., Zhu, J.Y., Torralba, A.: Rewriting a deep generative model. In: *Eur. Conf. Comput. Vis.* pp. 351–369. Springer (2020)
- [3] Bau, D., Zhu, J.Y., Strobel, H., Zhou, B., Tenenbaum, J.B., Freeman, W.T., Torralba, A.: GAN dissection: Visualizing and understanding generative adversarial networks. In: *Int. Conf. Learn. Represent.* (2019)
- [4] Boutsidis, C., Gallopoulos, E.: SVD based initialization: A head start for nonnegative matrix factorization. *Pattern Recognition* **41**(4), 1350–1362 (2008)
- [5] Broad, T., Leymarie, F.F., Grierson, M.: Network bending: Expressive manipulation of generative models in multiple domains. *Entropy* (2022)
- [6] Brock, A., Donahue, J., Simonyan, K.: Large scale GAN training for high fidelity natural image synthesis. In: *Int. Conf. Mach. Learn.* (2019)
- [7] Choi, Y., Uh, Y., Yoo, J., Ha, J.W.: Stargan v2: Diverse image synthesis for multiple domains. In: *IEEE Conf. Comput. Vis. Pattern Recog.* pp. 8188–8197 (2020)
- [8] Chong, M.J., Chu, W.S., Kumar, A., Forsyth, D.: Retrieve in style: Unsupervised facial feature transfer and retrieval. In: *Int. Conf. Comput. Vis.* (October 2021)
- [9] Cichocki, A., Zdunek, R., Phan, A.H., ichi Amari, S.: Nonnegative Matrix and Tensor Factorizations - Applications to Exploratory Multi-way Data Analysis and Blind Source Separation. Wiley (2009)
- [10] Collins, E., Achanta, R., Susstrunk, S.: Deep feature factorization for concept discovery. In: *Eur. Conf. Comput. Vis.* pp. 336–352 (2018)
- [11] Collins, E., Bala, R., Price, B., Süssstrunk, S.: Editing in style: Uncovering the local semantics of GANs. In: *IEEE Conf. Comput. Vis. Pattern Recog.* (2020)
- [12] Deng, J., Dong, W., Socher, R., Li, L.J., Li, K., Fei-Fei, L.: ImageNet: A large-scale hierarchical image database. In: *IEEE Conf. Comput. Vis. Pattern Recog.* pp. 248–255 (2009)
- [13] Ding, C., He, X., Simon, H.D.: On the equivalence of nonnegative matrix factorization and spectral clustering. In: *Proceedings of the 2005 SIAM international conference on data mining.* pp. 606–610. SIAM (2005)
- [14] Ding, C., Li, T., Peng, W., Park, H.: Orthogonal nonnegative matrix t-factorizations for clustering. In: *ACM SIGKDD Int. Conf. Knowledge Discovery and Data Mining. KDD '06*, Association for Computing Machinery, New York, NY, USA (2006)
- [15] Georgopoulos, M., Oldfield, J., Chrysos, G.G., Panagakis, Y.: Cluster-guided image synthesis with unconditional models (2021)
- [16] Goetschalckx, L., Andonian, A., Oliva, A., Isola, P.: Ganalyze: Toward visual definitions of cognitive image properties. In: *Int. Conf. Comput. Vis.* pp. 5744–5753 (2019)
- [17] Goodfellow, I., Pouget-Abadie, J., Mirza, M., Xu, B., Warde-Farley, D., Ozair, S., Courville, A., Bengio, Y.: Generative adversarial nets. In: *Adv. Neural Inform. Process. Syst.* (2014)
- [18] Haas, R., Graßhof, S., Brandt, S.S.: Tensor-based subspace factorization for StyleGAN. In: *Proc. Int. Conf. Automatic Face and Gesture Recognit. (FG)* (2021)
- [19] Haas, R., Graßhof, S., Brandt, S.S.: Tensor-based emotion editing in the StyleGAN latent space. In: *IEEE Conf. Comput. Vis. Pattern Recog. Worksh.* (2022)
- [20] Härkönen, E., Hertzmann, A., Lehtinen, J., Paris, S.: GANSpace: Discovering interpretable GAN controls. In: *Adv. Neural Inform. Process. Syst.* vol. 33, pp. 9841–9850 (2020)
- [21] He, Z., Kan, M., Shan, S.: Eigengan: Layer-wise eigen-learning for gans. In: *Int. Conf. Comput. Vis.* pp. 14408–14417 (2021)
- [22] Heusel, M., Ramsauer, H., Unterthiner, T., Nessler, B., Hochreiter, S.: GANs trained by a two time-scale update rule converge to a local nash equilibrium. *Adv. Neural Inform. Process. Syst.* **30** (2017)

- [23] Huang, X., Belongie, S.: Arbitrary style transfer in real-time with adaptive instance normalization. In: *Int. Conf. Comput. Vis.* (Oct 2017)
- [24] Jakoel, K., Efraim, L., Shaham, T.R.: GANs spatial control via inference-time adaptive normalization. In: *IEEE Winter Conf. Applic. Comput. Vis.* (January 2022)
- [25] Jayakumar, S.M., Czarnecki, W.M., Menick, J., Schwarz, J., Rae, J., Osindero, S., Teh, Y.W., Harley, T., Pascanu, R.: Multiplicative interactions and where to find them. In: *Int. Conf. Learn. Represent.* (2020)
- [26] Kafri, O., Patashnik, O., Alaluf, Y., Cohen-Or, D.: StyleFusion: A generative model for disentangling spatial segments (2021)
- [27] Karras, T., Aila, T., Laine, S., Lehtinen, J.: Progressive growing of GANs for improved quality, stability, and variation. In: *Int. Conf. Learn. Represent.* (2018)
- [28] Karras, T., Aittala, M., Hellsten, J., Laine, S., Lehtinen, J., Aila, T.: Training generative adversarial networks with limited data. *Adv. Neural Inform. Process. Syst.* **33**, 12104–12114 (2020)
- [29] Karras, T., Aittala, M., Laine, S., Härkönen, E., Hellsten, J., Lehtinen, J., Aila, T.: Alias-free generative adversarial networks. *Adv. Neural Inform. Process. Syst.* **34** (2021)
- [30] Karras, T., Laine, S., Aila, T.: A style-based generator architecture for generative adversarial networks. In: *IEEE Conf. Comput. Vis. Pattern Recog.* (June 2019)
- [31] Karras, T., Laine, S., Aittala, M., Hellsten, J., Lehtinen, J., Aila, T.: Analyzing and improving the image quality of StyleGAN. In: *IEEE Conf. Comput. Vis. Pattern Recog.* (June 2020)
- [32] Kim, H., Choi, Y., Kim, J., Yoo, S., Uh, Y.: Exploiting spatial dimensions of latent in gan for real-time image editing. In: *IEEE Conf. Comput. Vis. Pattern Recog.* (2021)
- [33] Kingma, D.P., Ba, J.: Adam: A method for stochastic optimization. *arXiv preprint arXiv:1412.6980* (2014)
- [34] Kolda, T.G., Bader, B.W.: Tensor Decompositions and Applications. *SIAM Review* **51**(3), 455–500 (Aug 2009)
- [35] Le, Q.V., Karpenko, A., Ngiam, J., Ng, A.Y.: ICA with Reconstruction Cost for Efficient Overcomplete Feature Learning. In: *Adv. Neural Inform. Process. Syst.* p. 9 (2013)
- [36] Lee, D.D., Seung, H.S.: Learning the parts of objects by non-negative matrix factorization. *Nature* **401**(6755), 788–791 (Oct 1999)
- [37] Li, T., Ding, C.: The relationships among various nonnegative matrix factorization methods for clustering. In: *Sixth International Conference on Data Mining (ICDM'06)*. pp. 362–371. *IEEE* (2006)
- [38] Lin, C.J.: Projected Gradient Methods for Nonnegative Matrix Factorization. *Neural Computation* **19**(10), 2756–2779 (Oct 2007)
- [39] Ling, H., Kreis, K., Li, D., Kim, S.W., Torralba, A., Fidler, S.: Editgan: High-precision semantic image editing. In: *Adv. Neural Inform. Process. Syst.* (2021)
- [40] Lu, H., Plataniotis, K.N., Venetsanopoulos, A.N.: MPCA: Multilinear principal component analysis of tensor objects. *IEEE Trans. Neural Networks* **19**(1), 18–39 (2008)
- [41] Olah, C., Satyanarayan, A., Johnson, I., Carter, S., Schubert, L., Ye, K., Mordvintsev, A.: The building blocks of interpretability. *Distill* (2018), <https://distill.pub/2018/building-blocks>
- [42] Oldfield, J., Georgopoulos, M., Panagakis, Y., Nicolaou, M.A., Patras, I.: Tensor Component Analysis for Interpreting the Latent Space of GANs. In: *Brit. Mach. Vis. Conf.* (Nov 2021)
- [43] Paszke, A., Gross, S., Massa, F., Lerer, A., Bradbury, J., Chanan, G., Killeen, T., Lin, Z., Gimelshein, N., Antiga, L., Desmaison, A., Kopf, A., Yang, E., DeVito, Z., Raison, M., Tejani, A., Chilamkurthy, S., Steiner, B., Fang, L., Bai, J., Chintala, S.: Pytorch: An imperative style, high-performance deep learning library. In: *Adv. Neural Inform. Process. Syst.*, pp. 8024–8035. *Curran Associates, Inc.* (2019)
- [44] Plumerault, A., Le Borgne, H., Hudelot, C.: Controlling generative models with continuous factors of variations. In: *Int. Conf. Learn. Represent.* (2020)
- [45] Rabin, J., Peyré, G., Delon, J., Bernot, M.: Wasserstein barycenter and its application to texture mixing. In: *Int. Conf. Scale Space and Variational Methods in Comput. Vis.* pp. 435–446 (2011)

- [46] Radford, A., Metz, L., Chintala, S.: Unsupervised representation learning with deep convolutional generative adversarial networks. In: *Int. Conf. Learn. Represent.* (2016)
- [47] Shen, Y., Gu, J., Tang, X., Zhou, B.: Interpreting the latent space of GANs for semantic face editing. In: *IEEE Conf. Comput. Vis. Pattern Recog.* (2020)
- [48] Shen, Y., Yang, C., Tang, X., Zhou, B.: InterFaceGAN: Interpreting the disentangled face representation learned by GANs. *IEEE Trans. Pattern Anal. Mach. Intell.* (2020)
- [49] Shen, Y., Zhou, B.: Closed-form factorization of latent semantics in GANs. In: *IEEE Conf. Comput. Vis. Pattern Recog.* (2021)
- [50] Suzuki, R., Koyama, M., Miyato, T., Yonetsuji, T., Zhu, H.: Spatially controllable image synthesis with internal representation collaging (2018)
- [51] Tucker, L.R.: Some mathematical notes on three-mode factor analysis. *Psychometrika* **31**(3), 279–311 (1966)
- [52] Tzelepis, C., Tzimiropoulos, G., Patras, I.: WarpedGANSpace: Finding non-linear RBF paths in GAN latent space. In: *Int. Conf. Comput. Vis.* pp. 6393–6402 (October 2021)
- [53] Voynov, A., Babenko, A.: Unsupervised discovery of interpretable directions in the GAN latent space. In: *Int. Conf. Mach. Learn.* pp. 9786–9796 (2020)
- [54] Wang, R., Chen, J., Yu, G., Sun, L., Yu, C., Gao, C., Sang, N.: Attribute-specific Control Units in StyleGAN for Fine-grained Image Manipulation. In: *ACM Int. Conf. Multimedia* (Oct 2021)
- [55] Wu, Z., Lischinski, D., Shechtman, E.: StyleSpace analysis: Disentangled controls for stylegan image generation. In: *IEEE Conf. Comput. Vis. Pattern Recog.* (2021)
- [56] Xu, D., Yan, S., Zhang, L., Zhang, H.J., Liu, Z., Shum, H.Y.: Concurrent subspaces analysis. In: *IEEE Conf. Comput. Vis. Pattern Recog.* vol. 2 (Jun 2005)
- [57] Yang, C., Shen, Y., Zhou, B.: Semantic hierarchy emerges in deep generative representations for scene synthesis. *Int. J. Comput. Vis.* **129**(5), 1451–1466 (2021)
- [58] Yang, Z., Laaksonen, J.: Multiplicative updates for non-negative projections. *Neurocomputing* **71**(1-3), 363–373 (2007)
- [59] Yang, Z., Oja, E.: Linear and nonlinear projective nonnegative matrix factorization. *IEEE Trans. Neural Networks* **21**(5), 734–749 (2010)
- [60] Yu, F., Seff, A., Zhang, Y., Song, S., Funkhouser, T., Xiao, J.: Lsun: Construction of a large-scale image dataset using deep learning with humans in the loop (2015)
- [61] Yuan, Z., Yang, Z., Oja, E.: Projective nonnegative matrix factorization: Sparseness, orthogonality, and clustering. *Neural Process. Lett* pp. 11–13 (2009)
- [62] Zhang, C., Xu, Y., Shen, Y.: Decorating your own bedroom: Locally controlling image generation with generative adversarial networks (2021)
- [63] Zhu, J., Feng, R., Shen, Y., Zhao, D., Zha, Z., Zhou, J., Chen, Q.: Low-Rank Subspaces in GANs. In: *Adv. Neural Inform. Process. Syst.* (2021)
- [64] Zhu, P., Abdal, R., Femiani, J., Wonka, P.: Barbershop: GAN-based Image Compositing using Segmentation Masks. *ACM Trans. Graph.* (Oct 2021)